ASIAN CONSORTIUM ACCMS–INTERNATIONAL CONFERENCE ICMG 2020

Nano-structured CuO on Silicon Using a Chemical Bath Deposition Process and Sputter Seed Layer

SHAMILI BANDARU,[1] CHANDRESWAR MAHATA,[2,6]
SABYASACHI CHAKRABORTTY,[1] SIDDHARTHA GHOSH,[3]
HASSAN ALGADI,[4] SEERAM RAMAKRISHNA,[5]
and GOUTAM KUMAR DALAPATI[3,5,7]

1.—Department of Chemistry, SRM University AP, Amaravati, Andhra Pradesh 522502, India. 2.—School of Electronics Engineering, Chungbuk National University, Cheongju 28644, Republic of Korea. 3.—Department of Physics, SRM University AP, Amaravati, Andhra Pradesh 522502, India. 4.—Department of Electrical Engineering, Faculty of Engineering, Najran University, P.O. Box 1988, Najran 11001, Kingdom of Saudi Arabia. 5.—Center for Nanofibers and Nanotechnology, Faculty of Engineering, National University of Singapore, Singapore 117576, Singapore. 6.—e-mail: chandreswar@gmail.com. 7.—e-mail: goutam.d@srmap.edu.in

Morphological changes of copper oxide (CuO) nano-structures have been studied in detail for renewable energy and electronic applications. The CuO nano-structures were grown on a silicon substrate via a two-stage process starting with radio frequency sputtering for the seed layer followed by chemical bath deposition. The study was focused on controlling the shape and size of the CuO nano-structures depending on various growth conditions, such as reaction time, growth temperature, and vertical/horizontal orientation of the substrate containing the sputtered-grown seed layer. Structural, optical, crystallographic, and morphological characteristics of the nano-structures were obtained through field-emission scanning electron microscopy, x-ray diffraction crystallographic analysis, and UV–Vis spectroscopy.

Key words: Nano-structures, copper oxide, sputtering seed layer, silicon substrate, growth temperature

INTRODUCTION

Transition metal oxide nano-structures have attracted significant attention in the nano-science and nano-technology research community due to their unique magnetic, optical, and electronic properties, which mainly depend on the morphology of the nano-structures. Various nano-structures of TiO_2, ZnO, Fe_2O_3, CuO have attracted significant attention due to being less toxic, cost-effective, and environmentally sustainable. Among them, copper is a very attractive element as it is earth-abundant, environmentally friendly, and of low cost. Copper oxide (CuO) nano-structures are very exciting for potential applications in the field of photo-voltaics,[1–3] photocatalysis,[4–6] gas sensors,[7–11] and as anti-bacterial agents.[12,13] Furthermore, CuO nano-structures are gaining widespread interest due to their high surface area, the ability for higher solar energy conversion, and high optical absorption with a tunable bandgap.[2]

CuO is a p-type semiconductor with its two different forms of copper oxides, $Cu_2O(I)$ oxide and $CuO(II)$ oxide. CuO has a bandgap in the range of $\sim$ 1.5–2.1, eV which is suitable for solar light-driven hydrogen production through water-splitting.[14,15] Also, high optical absorption with an adjustable bandgap of CuO-based photovoltaic devices has been previously demonstrated.[16,17] Masudy-panah et al. has investigated p-CuO (Ti)/ n-Si heterojunctions for solar cell applications with Ti doping within CuO.[18] It has been observed that

optimizing the Ti doping in CuO can increase the conductivity of the CuO (Ti), which results in an improvement of the short circuit current and the efficiency of p-CuO (Ti)/n-Si heterojunctions.[18] It is worth noting that, along with applications in solar absorbers, CuO has also been investigated in the field of anti-reflection coatings. Xia et al.[19] investigated copper oxide-based nano leaves to enhance silicon-based solar cell efficiency. A high surface to volume ratio and large surface conductivity with different shapes and sizes of CuO nano-structures have been found to be suitable for gas sensors, as shown by Yang et al.[11] CuO nano-structures can also be utilized for energy storage applications due to their optimal electrochemical property and higher specific capacitance.[20–22] Wang et al. showed that CuO thin films with network-like structures can be suitable candidates for negative electrodes in lithium batteries due to their capacitance of 560 mAh g^{-1} and long cyclic life.[23] Zhang et al.[24] has investigated the electrochemical properties os different shapes of CuO (nano-structures of cauliflower shape, nano-belts, and feather-shaped) synthesized by a chemical deposition method. Numerous methods have been adapted for the growth of CuO nano-structured thin films, such as a microwave-assisted hydrothermal method, a sol–gel method, a precipitation method, and a thermal–oxidation method.[25–30]

In the current work, we have proposed a simple, fast, and two-step synthesis procedure to tune nano-structures of CuO thin films. Different structures of CuO were synthesized using chemical bath deposition (CBD). The crystallinity, shape, and size were found to be tuned through the variation of the temperature, time, and orientation of the substrate during synthesis.

EXPERIMENTAL

Synthesis of CuO Nano-particle Thin Films

CuO nano-leave thin films were grown on silicon substrates via a two-step process. Initially, Si substrates, after successive cleaning with trichloroethylene, acetone, isopropyl alcohol, and de-ionized water, underwent consecutive ultra-sonication for 5 min to eliminate contaminants (metal or organic compounds) from them. Additionally, silicon samples were dipped into 1% hydrofluoric acid for 3 min to remove native silicon oxide. Silicon wafers were dried under nitrogen gas flow before loading into the chamber. A CuO nano-seed layer was deposited on the silicon substrate by sputtering of a stoichiometric CuO target (purity 99.999%) at a power of 50 W. The sputtering process for preparing the seed layers was carried out at a working pressure of 3.3 mTorr with an argon gas flow of 25 sccm for 5 min while keeping the substrate at room temperature. The second step involved the growth of various CuO nano-structured thin films on the seed layer, which was carried out via a CBD process. Growth solutions were prepared with an equimolar mixture of 0.025M [Cu (NO$_3$)$_2$·3H$_2$O] (copper nitrate trihydrate) and C$_6$H$_{12}$N$_4$-HMTA (hexamethylenetetramine) in deionized water. Figure 1 shows a schematic of the detailed CuO nano-structure synthesis process. To observe the modification of CuO nano-structures, the seed layer-coated samples were dipped horizontally and vertically into the solution under constant stirring. For the growth of different shaped and sized CuO nano-leaves, the bath solution was kept on a hot plate at temperatures of 80°C, 85°C, and 90°C for durations of 30 min, 60 min, 70 min, and 120 min. After deposition, the samples were cleaned with running de-ionized water to remove the residual solutes and impurities, and then dried by blowing nitrogen gas. Finally, the samples were
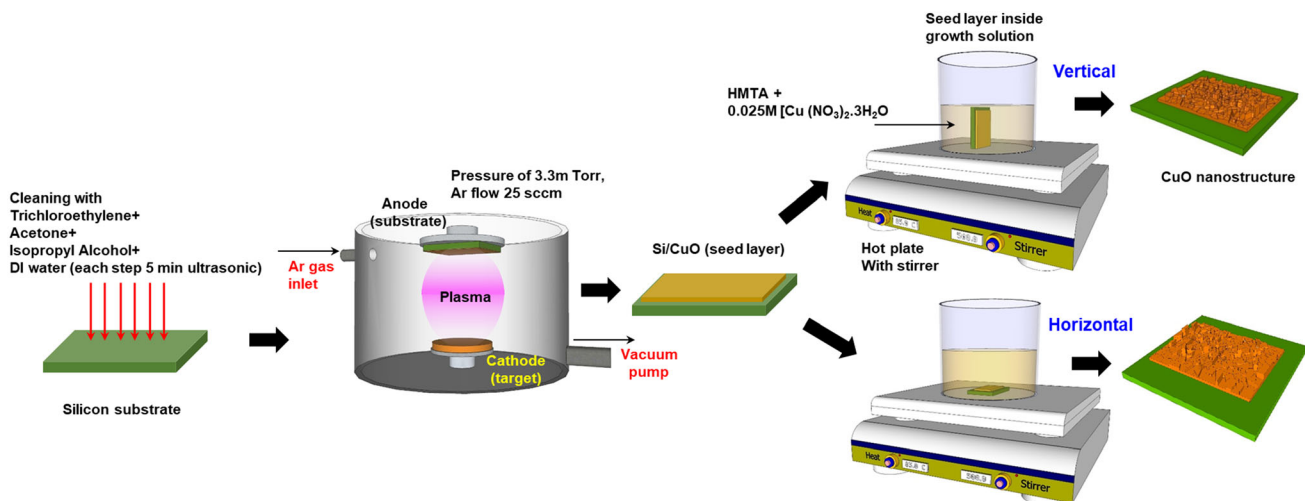

Fig. 1. Schematic of the two-step synthesis method of CuO nano-structures on Si substrates.

Table I. Different parameters followed during synthesis.

Sample	Concentration (molarity)	Temperature (°)	Time (min)	Orientation
S1	0.025	80	60	Vertical
S2	0.025	85	30	Vertical
S3	0.025	85	60	Vertical
S4	0.025	85	120	Vertical
S5	0.025	90	70	Vertical
S6	0.025	85	60	Horizontal

annealed at 400°C for 60 min in ambient air to enhance the crystal quality of the films. Structural surface morphology and crystallography identification of the CuO nano-leave thin films were analyzed by x-ray diffraction (XRD) using a Bruker AXS general area detector diffraction system, and field-emission scanning electron microscopy (FESEM) (JEOL FESEM JSM 6700F). Table I shows the experimental conditions to synthesize the CuO nano-structures with different shapes and sizes.

RESULTS AND DISCUSSION

The description of the growth kinetics of CuO nano-leaves with different morphologies obtained when copper(II) nitrate trihydrate and HMTA were reacted in a chemical bath are as follows. HTMA produces NH_3 and DI water initially produces oxygen, which leads to the formation of NH_4^+ and OH^- ions, which react with the copper nitrate present in the bath solution, leading to the formation of ammonia nitrate and copper hydroxide nano-particles. The nucleation process was initiated by $Cu(OH)_2$ nano-particles, producing polycrystalline $Cu(OH)_2$ nano-wires due to agglomeration, and they undergo an orientation attachment process leading to the formation of single-crystal $Cu(OH)_2$ nano-leaves by reconstructive transformation.[31] Increasing the CBD time and temperature, this transitional development of copper hydroxide is changed to solid-state CuO thin films by dehydration. For a nano-particle to combine with the substrate to form a thin film, a supersaturated solution is required in the chemical bath during deposition.[32] Figure 2 shows the XRD patterns of the crystallographic phase in CuO nano-structures synthesized at 85°C for 30 min and 120 min. The copper atoms with coordination number 4 bind to the neighboring oxygen atoms in a roughly square planar design in the (110) plane.[33] The presence of multiple XRD peaks at 25.73°, 32.09°, 33.69°, 36.52°, 38.34°, 41.94°, 43.57°, 49.21°, 53.42°, 58.15°, 60.78°, 62.72°, and 70.48° was evident, which could be indexed to the monoclinic crystallite phase of CuO and assigned to the (021), (110), (002), (111), (042), (130), (131), (151), (113), (200), (152), and (202) crystalline plane. This is in good agreement with the standard database (JCPDS File no: 5-0661). The
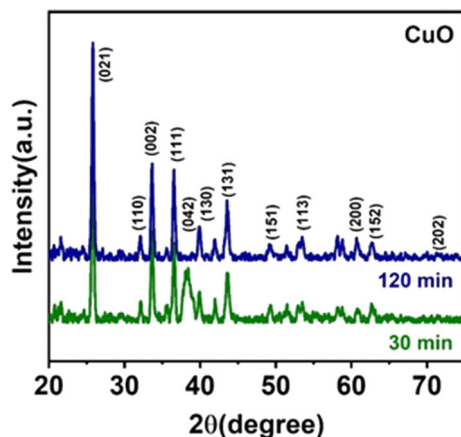

Fig. 2. XRD patterns for CuO nano-structures at a growth temperature of 85°C for 30 min and 120 min.

prominent peak for the XRD pattern was calculated using Scherrer's formula:

$$D = \frac{0.9\chi}{\beta Cos\theta} \quad (1)$$

where D is the crystalline size, χ the wavelength of the x-ray, β is the full width at half maximum of the prominent peak for CuO, and θ is the diffracting angle. The grain size of the nano-structure synthesized for 30 min was 51.77 nm (using Eq. 2) whereas the grain size for the nano-structure synthesized for 120 min was 53.69 nm (using Eq. 3):

$$D = \frac{0.9(0.154)}{(0.0028).(0.956)} \quad D = 51.77\,nm \quad (2)$$

$$D = \frac{0.9(0.154)}{(0.0027).(0.956)} \quad D = 53.69\,nm \quad (3)$$

From Fig. 2, it can be seen that the intensity of the different peaks increased along with the reaction time which is due to the increase in the thickness of the thin films due to effective mass transfer during the long reaction.

UV-Vis optical transmittance spectra were studied to determine the bandgap of CuO nano-structures under the as-deposited and annealed conditions. From the transmission spectra, it was
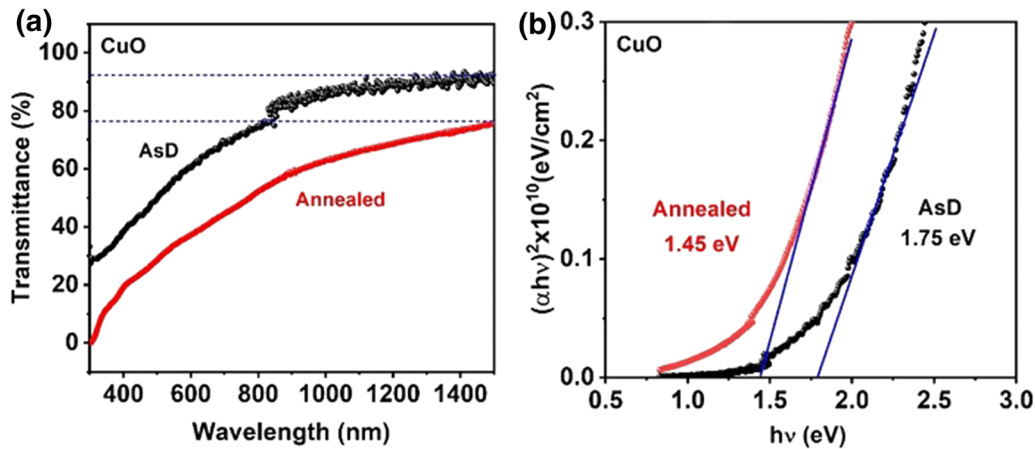
Fig. 3. (a) Optical transmission spectra of CuO nano-structures for as-deposited and annealed conditions (b) The CuO nano-structure bandgap, obtained from Tauc plots.

revealed that visible absorption was significantly enhanced after thermal treatment of the CuO nano-structures, as shown in Fig. 3a. The optical band gap under different conditions was evaluated by Tauc plots, as shown in Fig. 3b. From Eq.

$$(\alpha h v)^2 \propto (h v - E_{(g)}) \qquad (4)$$

$h v$ is the photon energy, α is the absorption coefficient, h is Plank's constant, and E_g is the bandgap. So, from the extrapolation of the straight line on the $(\alpha h v)^2$ versus $h v$ plot, bandgaps of 1.75 eV and 1.45 eV were obtained for as-deposited and annealed samples, respectively. The results are in good agreement with previously reported results.[19,31] Band gap lowering for annealed sample may be due to the predominant phase change from Cu_2O to CuO which indicates better oxidation states.[34] After annealing, oxygen vacancies in CuO were significantly reduced as a result, and density of the vacant lattice and the lattice order decreased.

Field-Emission Scanning Electron Microscopy (FESEM)

Nano-structured thin films were synthesized under different experimental conditions in vertical and horizontal orientations of the CuO-seeded sample. Nano-structure size and morphology were studied by using FESEM, which illustrates the CuO nano-structures which were self-organized as nano-leaves. To study the tunability in the morphology of CuO nano-structures, the experiment was conducted for 30 min, 60 min, and 120 min. Figure 4 depicts the morphological changes at different reaction times.

Figure 4a–d shows the FESEM images of CuO nano-structures after carrying out the reactions for 30 min, 60 min, and 120 min at 85°C temperature with the CuO seeded sample placed in a vertical position. It is evident from Fig. 4–c that the nano-structured CuO thin films grown for 30 and 60 min

are self-assembled in the form of nano-leaves. An average nano-structure size of ~ 562 nm with a standard deviation (SD) of ~ 200 nm was observed for the nano-structures grown for 30 min, while it was 670 nm with a SD of ~ 161 nm for the nano-structures grown for 60 min at 85°C. The nano-structures grown for 30 min and 60 min are similar. Figure 4d shows nano-structures grown for 120 min under the same reaction conditions. Due to the increased time of reaction, the particles undergo uneven growth and the average size of the nano-structures increases to 1758.5 nm. CuO nano-structures grown for 60 min and 120 min have a thickness of 95.4 nm and 277 nm, respectively. It is worth noting that the thickness of the nano-structure grown for 30 min was 48.3 nm. Thus, it is very important to control the reaction time to achieve nano-leaves with uniform distribution. The nano-structures size increment was due to the increase in grain size with an increase of time from 60 min to double the reaction time, up to 120 min.[35] The increased size of the particles is summarized in Table II.

In general, the nano-structure size increases with an increase in temperature due to two main reasons. One is the oriented attachment of the primary nano-particles and the second is Ostwald ripening.[31] The reaction mechanism and nano-structure formation also depend on the orientation of the sputtered CuO-seeded samples. CuO nano-structure morphology was also studied for the films grown with the seeded layer placed in the horizontal and vertical positions. Supplementary Fig. S1 shows the nano-structures of the thin films grown at a fixed temperature and time with variation in the orientation of the growth samples. The temperature of the bath and the reaction time were fixed at 85°C and 60 min, respectively, for both samples. CuO nano-structures are irregular in shape and the nano-structure size ranges up to 652.3 nm with a thickness of 100.3 nm when the experiment was carried out with the seeded layer placed in the
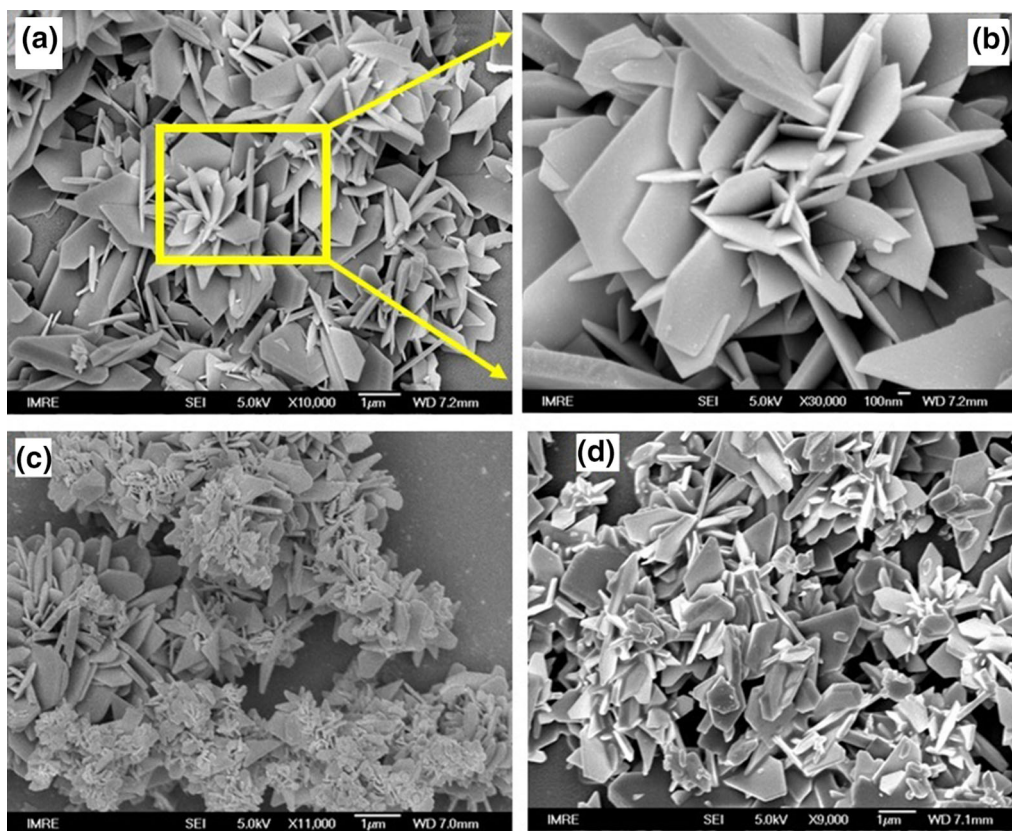
Fig. 4. FESEM images of CuO nano-structures grown at 85°C for (a) 30 min, (c) 60 min, and (d) 120 min; (b) is a high-resolution image of (a).

Table II. Representations of morphological changes with changes in the time of reaction

Sample	Concentration (molarity)	Temperature (°)	Time (min)	Orientation	Average length (nm)	SD	Width (nm)
S2	0.025	85	30	Vertical	562.2	200.3	48.3
S3	0.025	85	60	Vertical	670.0	161.6	95.4
S4	0.025	85	120	Vertical	1758.5	422.6	277.0

Table III. CuO nano-structure properties depending on the orientation of the CuO-seeded sample in the chemical bath

Sample	Concentration (molarity)	Temperature (°)	Time (min)	Orientation	Length (nm)	SD	Width (nm)
S3	0.025	85	60	Vertical	691.4	209.6	84.3
S6	0.025	85	60	Horizontal	652.3	176.8	100.3

horizontal direction (see supplementary Fig. S1). However, as mentioned earlier, the particles are 691.4 nm size with a thickness of 84.3 nm when the reaction was carried out by placing the seeded layer in the vertical direction, as shown in supplementary Fig. S1b. CuO nano-structure properties with the different orientations of the CuO-seeded sample are summarized in Table III.

The structural transformation of spherical nano-particles to nano-leaves is shown in supplementary Fig. S2. It can be seen from Fig. S2a that the particles are growing like a bunch of nano-leaves with each leaf structure size up to 546.4 nm whereas the overall width of nano-bunch is 106 nm when the reaction was carried out at 80°C for 60 min in the vertical orientation of the silicon wafer (Table IV). In parallel, the increment of

Table IV. CuO nano-structure sizes with variation of the growth temperature and reaction time of (a) 80°C, 60 min, (b) 90°C, 70 min, and (c) 85°C, 30 min

Sample	Concentration (molarity)	Temperature (°)	Time (min)	Orientation	Length (nm)	SD	Width (nm)
S1	0.025	80	60	Vertical	546.4	120.5	106.0
S5	0.025	90	70	Vertical	362.7	91.0	72.7
S2	0.025	85	30	Vertical	562.2	200.3	48.3

temperature and reaction time, as shown in supplementary Fig. S2b, asymmetric and polydispersed nano-leaves were formed with a size of 362.7 nm with 72.7 nm thickness. On the other hand, when the samples were placed vertically at 85°C for 30 min, the CuO nano-structures are highly monodispersed with a nano leaf size of 562.2 nm and thickness of 48.3 nm, as shown in supplementary Fig. S2c and Table IV. From the FESEM micrographs, it has been confirmed that the nano-structures are systematically organized in the form of leaves. This phenomenon is due to the influence of internal stress inside the solution bath during the chemical reaction of the growth process of the film. Atom arrangements in the chemical bath were dominated by the internal stress that may be acquired due to some external parameters during the film growth. Hence, we can observe the leaf-like morphology by the simple strategy of the experimental variation of the temperature and the time of reaction in the chemical bath.

CONCLUSIONS

CuO nano-structure tunability was studied in detail by synthesizing thin films using an ultra-thin sputter-grown seed layer followed by CBD with different reaction times, synthesis temperatures, and orientations of the silicon substrate. The samples were characterized using scanning electron microscopy to find a systematic microscopic morphology of these CuO nano-leaf structures. CuO nano-leaves were found to be in the monoclinic crystallographic phase, which was confirmed by the XRD patterns. The size of the nano-structures depends on the reaction parameters. Reaction times and temperatures are crucial to tune the CuO nano-leaf size. This work shows a synthesis route of highly crystalline CuO nanoleaves using sputter-grown seed and CBD.

CONFLICT OF INTEREST

The authors declared that they have no conflict of interest.

SUPPLEMENTARY INFORMATION

The online version contains supplementary material available at https://doi.org/10.1007/s11664-021-08772-4.

REFERENCES

1. O. Langmar, E. Fazio, P. Schol, G. de la Torre, R.D. Costa, T. Torres, and D.M. Guldi, *Angew. Chem. Int. Ed.*, 2019, **58**(12), 4056.
2. S. Masudy-Panah, S. Zhuk, H.R. Tan, X. Gong, and G.K. Dalapati, *Nano Energy*, 2018, 46, 158.
3. Q. Sun, S. Zhou, X. Shi, X. Wang, L. Gao, Z. Li, and Y. Hao, *ACS Appl. Mater. Interfaces*, 2018, 10(13), 11289.
4. Q. Chen, D. Liu, B. Cao, Z. Wang, T. Wang, B. Wang, Z. Wang, Y. Yang, X. Xiong, and Y. Wang, *J. Electron. Mater.*, 2020, 49(3), 2032.
5. N.C. Khang, *J. Electron. Mater.*, 2017, 46(10), 5497.
6. K. Sahu, S. Choudhary, S.A. Khan, A. Pandey, and S. Mohapatra, *Nano-Struct. Nano-Objects*, 2019, 17, 92.
17. G. Peng, S. Wu, J.E. Ellis, X. Xu, G. Xu, C. Yu, and A. Star, *J. Mater. Chem. C*, 2016, 4(27), 6575.
8. H. Zhang, H. Li, L. Cai, Q. Lei, J. Wang, W. Fan, K. Shi, and G. Han, *J. Mater. Sci. Mater. Electron.*, 2020, 31(2), 910.
9. W. Andrysiewicz, J. Krzeminski, K. Skarżynski, K. Marszalek, M. Sloma, and A. Rydosz, *Electron. Mater. Lett.*, 2020, 16(2), 146.
10. S. Ganguly, R. Jha, P.K. Guha, and C. Jacob, *J. Electron. Mater.*, 2020, 49, 5070.
11. C. Yang, X. Su, J. Wang, X. Cao, S. Wang, and L. Zhang, *Sensors Actuators B*, 2013, 185, 159.
12. S. Meghana, P. Kabra, S. Chakraborty, and N. Padmavathy, *RSC Adv*, 2015, 5(16), 12293.
13. M. Hans, A. Erbe, S. Mathews, Y. Chen, M. Solioz, and F. Mücklich, *Langmuir*, 2013, 29(52), 16160.
14. A. Cots, P. Bonete, and R. Gómez, *ACS Appl. Mater. Interfaces*, 2018, 10(31), 26348.
15. S. Masudy-Panah, K. Radhakrishnan, A. Kumar, T.I. Wong, R. Yi, and G.K. Dalapati, *J. Appl. Phys.*, 2015, 118, 225301.
16. C. de Melo, M. Jullien, Y. Battie, A. En Naciri, J. Ghanbaja, F. Montaigne, and S. Migot, *ACS Appl. Nano Mater.*, 2019, 2(7), 4358.
17. W. Liao, Y. Gao, W. Wang, X. Zuo, Q. Yang, Y. Lin, H. Tang, S. Jin, and G. Li, *ACS Sustain. Chem. Eng.*, 2020, 8(19), 7308.
18. S. Masudy-Panah, K. Radhakrishnan, H.R. Tan, R. Yi, T.I. Wong, and G.K. Dalapati, *Sol. Energy Mater. Sol. Cells*, 2015, 140, 266.
19. Y. Xia, X. Pu, J. Liu, J. Liang, P. Liu, X. Li, and X. Yu, *J. Mater. Chem. A*, 2014, 2(19), 6796.
20. N.A. Niaz, F. Hussain, R.M.A. Khalil, M. Imran, A. Shakoor, N.R. Khalid, B. Choudhry, M.A. Khan, and S. Kim, *J. Electron. Mater.*, 2020, 49(2), 1096.
21. X. He, and J. Bae, *J. Electron. Mater.*, 2018, 47(9), 5468.
22. J. Zhou, L. Ma, H. Song, B. Wu, and X. Chen, *Electrochem. Commun.*, 2011, 13(12), 1357.
23. H. Wang, Q. Pan, J. Zhao, G. Yin, and P. Zuo, *J. Power Sources*, 2007, 167(1), 206.
24. H. Zhang, and M. Zhang, *Mater. Chem. Phys.*, 2008, 108(2–3), 184.
25. K. Sahu, A. Bisht, S.A. Khan, A. Pandey, and S. Mohapatra, *Ceram. Int.*, 2020, 46(6), 7499.
26. M. Zahan, and J. Podder, *SN Appl. Sci.*, 2020, 2(3), 385.
27. S.P. Ashokkumar, H. Vijeth, L. Yesappa, M. Niranjana, M. Vandana, and H. Devendrappa, *Inorgan. Chem. Commun.*, 2020, 115, 107865.

28. M. Makenali, I. Kazeminezhad, *Inorgan. Nano-Met. Chem.*, 2020, 50, 1.
29. R. Singh, L. Yadav, and T. Shweta, *Thin Solid Films*, 2019, 685, 195.
30. L. Yin, H. Wang, L. Li, H. Li, D. Chen, and R. Zhang, *Appl. Surf. Sci.*, 2019, 476, 107.
31. C.L. Londoño-Calderón, S. Menchaca-Nal, N.J. François, L.G. Pampillo, and P. Froimowicz, *ACS Appl. Nano Mater.*, 2020, 3(3), 2987.
32. J. Sultana, S. Paul, A. Karmakar, R. Yi, G.K. Dalapati, and S. Chattopadhyay, *Appl. Surf. Sci.*, 2017, 418, 380.
33. C. Tamuly, I. Saikia, M. Hazarika, and M.R. Das, *RSC Adv.*, 2014, 4(95), 53229.
34. F. Du, Q.Y. Chen, and Y.H. Wang, *J. Phys. Chem. Solids*, 2017, 104, 139.
35. P. Vinothkumar, C. Manoharan, B. Shanmugapriya, and M. Bououdina, *J. Mater. Sci. Mater. Electron.*, 2019, 30(6), 6249.